Journal of Power Sources 206 (2012) 267–273

Contents lists available at SciVerse ScienceDirect

Journal of Power Sources

journal homepage: www.elsevier.com/locate/jpowsour

Fabrication of Si core/C shell nanofibers and their electrochemical performances as a lithium-ion battery anode

Byoung-Sun Lee[a], Seoung-Bum Son[a,b], Kyu-Min Park[a], Jong-Hyun Seo[e], Se-Hee Lee[b,c], In-Suk Choi[d], Kyu-Hwan Oh[a], Woong-Ryeol Yu[a,*]

[a] Department of Materials Science and Engineering, Seoul National University, 599 Gwanangno, Gwanak-gu, Seoul 151-742, Republic of Korea
[b] Department of Mechanical Engineering, University of Colorado 427 UCB, Boulder, CO 80309, USA
[c] World Class University Hybrid Materials Program, Department of Materials Science and Engineering, Seoul National University, 599 Gwanangno, Gwanak-gu, Seoul 151-742, Republic of Korea
[d] High Temperature Energy Center, Korea Institute of Science and Technology, Seoul 136-791, Republic of Korea
[e] Advanced Analysis center, Korea Institute of Science and Technology, Seoul 136-791, Republic of Korea

ARTICLE INFO

Article history:
Received 22 November 2011
Received in revised form 3 January 2012
Accepted 6 January 2012
Available online 28 January 2012

Keywords:
Si core/C shell nanofibers
Co-axial electrospinning
Buffering effect
Electrochemical performance

ABSTRACT

This paper reports on Si core/C shell nanofibers as an anode material for Li-ion batteries. The Si core/C shell nanofibers are synthesized using co-axial electrospinning of Si nanoparticles in styrene-*co*-acrylonitrile core solution and poly(acrylonitrile) shell solution combined with subsequent thermal treatments. The microstructure and elemental composition of the nanofibers are systematically examined using FE-SEM, TEM and WAXD for confirmation of the crystalline Si core/turbostratic C shell structure. In situ observation of contact-lithiation of the Si core/C shell nanofibers is carried out to investigate their mechanical durability during the electrochemical reactions. The electrochemical performances of the nanofibers as an anode are characterized by galvanostatic charge–discharge test. Due to simple processing but a well-developed core/shell structure and good electrochemical performance, the Si core/C shell nanofibers fabricated in this study offer the potential to develop enhanced Si/C nanostructured composite anodes.

1. Introduction

Since the early 1990s, lithium-ion batteries (LIB) have been most widely utilized as power sources for various commodities, ranging from portable electronic devices to electric (or hybrid) vehicles. There is a growing demand on advanced LIBs with higher specific capacity and longer cycling performance. Commercialized anodes (graphitic carbon), however, have been obstacles to achieving this because of their low specific capacity (i.e., 372 mAh g^{-1}), promoting various and vast research towards advanced LIBs, in particular anode materials [1].

Silicon has emerged as a promising anode material due to its huge theoretical specific capacity (4200 mAh g^{-1}) and low working potential (about 0.5 V vs Li/Li^+) [2]. Si anodes have shown, however, critical limitations due to large volume expansion (400%) and thus pulverization and electrical contact loss during lithiation and delithiation processes [3]. In order to overcome the aforementioned demerits, many research have been dedicated to understanding the lithiation behavior of silicon anodes using various methods such as ab initio calculation [4], critical size determination of silicon anodes [5], in situ lithiation observation of single nanowire filaments in HR-TEM [6,7], ex situ observation of single crystalline nanowires [8], and ex situ microstructural analyses on silicon particles [2]. Now it is the common knowledge that the crystalline Si nanomaterials undergo anisotropic volume expansion along the preferential direction (i.e., ⟨1 1 0⟩) and amorphization during the lithiation. Then, they are finally transformed to amorphous lithium silicide with significant volume expansion compared to their pristine form.

Many researchers have developed novel structured silicon anodes: three-dimensional porous particles [9,10], hollow nanospheres [11], nanowire arrays [12,13], nanotube arrays [1,14], crystalline core/amorphous shell nanowires [15], combination with various types of carbonaceous materials [16–21], and silicon oxide compounds [22]. Among these efforts, the combination of silicon and carbon is regarded as a very fascinating method because of the mutual compensation of their weaknesses, i.e., the low specific capacity of carbon and the mechanical instability and electrical contact loss of silicon. Thus, a great number of carbonaceous materials have been composited with silicon for advanced anode materials. Related previous works can be classified mainly by the types of carbon (soft [21,23] and hard [17,20,24] carbon) and structural dimensions such as particles (zero or three-dimensional) [19],

* Corresponding author. Tel.: +82 2 880 9096; fax: +82 2 883 8197.
E-mail address: woongryu@snu.ac.kr (W.-R. Yu).

0378-7753/$ – see front matter © 2012 Elsevier B.V. All rights reserved.
doi:10.1016/j.jpowsour.2012.01.120

wires (one-dimensional) [25–27], and films (two-dimensional) [21]. They can be also classified by compositing types: simple mixture [20,25,26,28] and core/shell types [16,27]. The simple mixtures offer relatively simple processing methods and thus improve the feasibility of mass-production; however their electrochemical performances (low specific capacity and retention) need to be improved. Recently, poly(acrylonitrile) (PAN)-based electrospun silicon/carbon mixed nanofibers have been studied because of processing convenience as well as better specific capacities than commercial graphite [26,28–32].

Meanwhile, the core/shell types have shown excellent electrochemical performances, yet productivity is generally not feasible due to the complex processing. The co-axial electrospinning process has been frequently employed to fabricate the core/shell structured nanofibers [33–35], for example, Sn core/C shell nanofibers and soft carbon core/hard carbon shell nanofibers [33,35]. In this work, Si core/C shell nanofibers are prepared using a simple processing method to investigate their contact-lithiation behavior, to assess their electrochemical performances, and finally to demonstrate that the Si core/C shell nanofibers are promising anode materials satisfying both productivity and electrochemical performances.

2. Experimental

2.1. Precursor nanofibers preparation

PAN (M_w = 200,000 g mol^{-1}, Misui chemical) is used as a carbonizing precursor in the shell solution. Styrene-co-acrylonitrile (SAN, AN 28.5 mol%, M_w = 120,000 g mol^{-1}, Cheil industries) is used as the sacrificial core material carrying Si nanoparticles. SAN and PAN are commonly dissolved in *N*,*N*-dimethylformamide (DMF, purity 99.5%, Daejung chemical) and their concentrations are set to be 30 and 20 wt.%, respectively. Each solution is then ultrasonicated for 5 h, and further stirred at 80 °C for 5 h. Si nanoparticles (0.5 g, D < 100 nm, Aldrich) are added to SAN solution (10 g), which is further stirred at 80 °C for 5 h.

A co-axial nozzle with two concentric cylinders has been designed to make core/shell precursor nanofibers. The gauge numbers of the needles are 17 and 22 for outer and inner cylinders, respectively. The co-axial electrospinning conditions are set up as follows: applied voltage – 18 kV, tip-to-collector distance – 15 cm, the flow rates of the inner and outer solutions – 0.5 and 1 ml h^{-1}, respectively. SAN core/PAN shell co-axial electrospun nanofibers without Si nanoparticles was also prepared using the same electrospinning conditions to make pure hollow carbon nanofibers [36].

2.2. Thermal treatment

Core (SAN + Si)/shell (PAN) precursor nanofibers are then thermally treated for the stabilization and carbonization of the PAN shell. The thermal treatment is mainly concentrated on the conversion of raw PAN into the turbostratic carbon, during which the sacrificial core (SAN) is burnt out, leaving Si nanoparticles in the core. The stabilization of the PAN shell is carried out at 270–300 °C for 1 h under the air atmosphere, and the subsequent carbonization is carried out at 1000 °C for 1 h under the nitrogen atmosphere. Here the temperature is increased at a rate of 10 °C min^{-1}.

2.3. Characterizations

The morphologies and atomic composition of the Si core/C shell nanofibers are investigated using a field emission scanning electron microscope (FE-SEM) (SUPRA 55VP, Carl Zeiss). The Si core/C shell structure is investigated using a high resolution transmission electron microscope (HR-TEM, JEM-3000F). Wide angle X-ray diffraction (WAXD) (wave length: 0.154 nm, New D8 Advance, Bruker) are employed to characterize the carbonized samples.

2.4. In situ contact-lithiation

The contact-lithiation behavior of a Si core/C shell nanofiber when contacted on the fresh Li metal is conducted and recorded by using Focused Ion Beam (FIB, QANTA3D, FEI Co.). The Si core/C shell nanofiber is attached to the tungsten tip of the nanomanipulator (MM3A, Kleindiek). The nanofiber is cut by FIB at the middle of the bead into a bell-shaped pouch for observing Si-rich part. The Li metal is cut in the glove box under Ar gas and moved to FIB without oxidation. The expansions of Si and C during contact-lithiation are calculated by using Image J software.

2.5. Electrochemical characterization

A two-electrode 2032-type coin capsule is employed to assess the electrochemical performances of the Si core/C shell nanofibers [37]. The anode slurry is prepared by mixing Si core/C shell nanofibers (60 wt.%), acetylene black (20 wt.%, Alfa Aesar), and poly(vinylidene floride) (20 wt.%, Alfa Aesar) in 1-methyl-2-pyrrolidinone (Alfa Aesar). The slurry is then screen-printed onto a copper foil (Alfa Aesar) and dried. The mass of Si core/C shell nanofibers in anode is 0.990 mg, while the surface area is 0.01889 m^2, which is indirectly calculated based on the BET surface area of 19.077 m^2 g^{-1}. The actual amount of anode materials in this test is small, and thus the results may not be extrapolated for scale-up, e.g., commercialized cell sized sample. The results, however, can be interpreted as the maximum performance of the electrode materials because the current test cell excludes any size effects involved in mass manufacturing. A lithium foil (Alfa Aesar) is used as the counter and reference electrode for a half-cell configuration. Glass fibers (Whatman) are used as the separator, while 1 M $LiPF_6$ in a mixed solution of propylene carbonate and diethyl carbonate (volume ratio 1:1, TSC Michigan) is used for the electrolyte. The coin-capsule is assembled, crimped, and closed in an Ar-filled glove box. The electrochemical performance is then investigated at a current density of 50 mA g^{-1} for lithium insertion and extraction between 0.01 and 1.5 V.

3. Results and discussion

3.1. Fabrication of Si core/C shell nanofibers

Fig. 1(a) shows a schematic illustration of the co-axial electrospinning setup. The Si nanoparticles dispersed SAN solution (core) is vertically supplied, while the PAN solution (shell) is horizontally fed. The co-axial electrospinning process is much more complicated than single solid nozzle electrospinning, because the differences between core and shell properties (for example, conductivities and viscosities of each fluids and miscibility between/among fluids) allow very narrow processing window for stable electrospinning. In the authors' previous work, it was found that a SAN core/PAN shell combination is highly suitable to make hollow carbon nanofibers for several reasons: the non-precipitation between core and shell solutions by a common solvent (DMF), immiscibility between the two solutions, the large conductivity difference between core (lower) and shell (higher) solutions, and the different metamorphoses during thermal treatment [36]. In this work, the aforementioned system is employed to make Si core/C shell nanofibers. Fig. 1(b) schematically shows the transformation of Si nanoparticles dispersed SAN core/PAN shell nanofibers to Si core/C shell nanofibers by thermal treatment. During the stabilization process in the air atmosphere, SAN core carrying Si nanoparticles becomes molten, while PAN in the shell

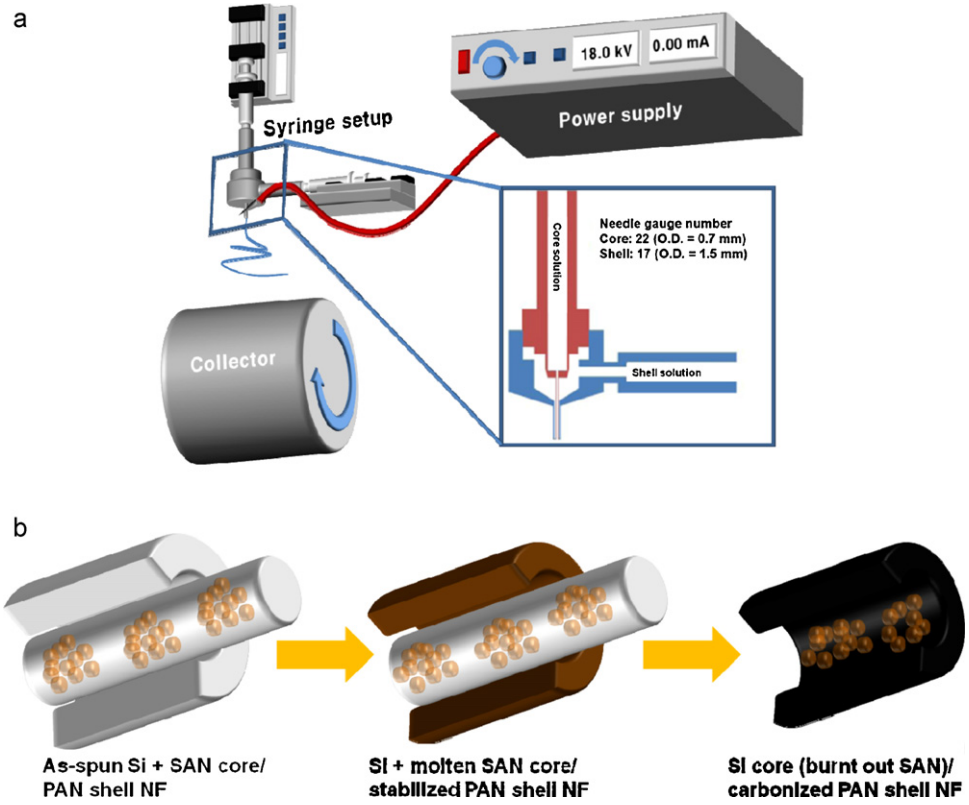

Fig. 1. Schematic illustrations of: (a) co-axial electrospinning system and (b) structural change during thermal treatment. 'NF' represents *nanofibers*.

is transformed to the stabilized structure via cyclization and dehydrogenation [38]. Further thermal treatment burns out the molten SAN and carbonizes the stabilized PAN, leaving Si nanoparticles in hollow carbon nanofibers. Note that Si nanoparticles remain intact without any chemical transformation during the thermal treatment.

Fig. 2(a) shows the Si core/C shell nanofibers prepared by the aforementioned process. The nanofibers consist of smooth strings and repeated beads like "beads on string". The average diameters of the string and bead are 930 nm (±82 nm) and 1287 nm (±245 nm), respectively, and this difference in the diameter clearly represents the incorporated Si nanoparticles. Note that the beads are much less conspicuous than those in previous works [25,28], because molten and burnt-out SAN give mobility to the lumps of Si nanoparticles during the thermal treatment. The high resolution SEM image in Fig. 2(b) shows Si nanoparticle core and carbonized PAN shell in a cross-section of Si core/C shell nanofibers. Fig. 3(a) also supports the discrete Si nanoparticles core/carbonized PAN shell (Si core/C shell) structure. The energy dispersive X-ray spectroscopy (EDX) profile in Fig. 3(b) clearly demonstrates that the nanofibers mainly consist of C and Si. The miscellaneous peaks for O and Cu can be observed: O atoms are included during the stabilization process, while Cu comes from the observation grid. The quantitative weight ratio of C and Si in the uniform nanofibers is found out to be 9.1:1 according to the EDX profile from FE-SEM (see Fig. 4). The intended ratio of C and Si is 5.36:1 in the solution preparation, implying that the Si proportion is lowered during the electrospinning process by drop formations.

Fig. 5 shows that the Si core remains in a crystalline phase after the thermal treatment, while the PAN shell is transformed into a carbonized structure. WAXD curve shows two broad and seven sharp peaks: (0 0 2) and (1 0 1) for the turbostratic carbon and (1 1 1), (2 2 0), (3 1 1), (4 0 0), (3 3 1), (4 2 2), and (5 1 1) for the crystalline Si [28,39]. The d_{002} value of the carbonized shell is calculated to be 0.369 nm, which is greater than that of graphite (0.335 nm). It implies that the microstructure of the shell is transformed to carbonaceous structure with a slightly mismatched layer-sequence [36,40]. Meanwhile, the sharp peaks in Fig. 5 demonstrate that the crystalline phase of Si is maintained without any chemical reactions during thermal treatment. Thus, it can be claimed that the crystalline Si core/turbostratic C shell nanofibers have been successfully fabricated.

3.2. *In situ observation of contact-lithiation*

In situ deformation behavior of the Si core/C shell nanofibers during the lithiation process has been investigated using a novel contact-lithiation method. Fig. 6(a) shows the morphological images of the Si core/C shell nanofibers before and after the contact-lithiation. The bell-shaped pouch and the small particles in the images represent the C shell and the Si core nanoparticles, respectively. The schematic sequence of in situ contact-lithiation behavior of a Si core/C shell nanofiber is described in Fig. 7(a) (see a supplementary movie S1 for actual experiment). When the nanofiber contacts on the Li metal, the contact-lithiation starts, i.e., Li atoms inter-diffuse into both the C shell and Si core nanoparticles due to its chemical potential gradient. Li atoms in the C shell then intercalate into among turbostratic carbon layers, while Li atoms in the Si core nanoparticles ionize to minimize their potential energy in Si matrix, thereby they alloy with the crystalline Si (see Fig. 7(b) for the schematic explanation) [41]. The Li-ion moves into the Si matrix because of the concentration gradient, while the electron is injected to the conduction band of Si because of the electron poverty of Si matrix [42].

The length change of the C shell in the circumferential direction is measured to be 1.49%. No mechanical failure is observed because the PAN-derived carbon nanofibers show improved modulus and strength with their breaking elongation (~2%) being

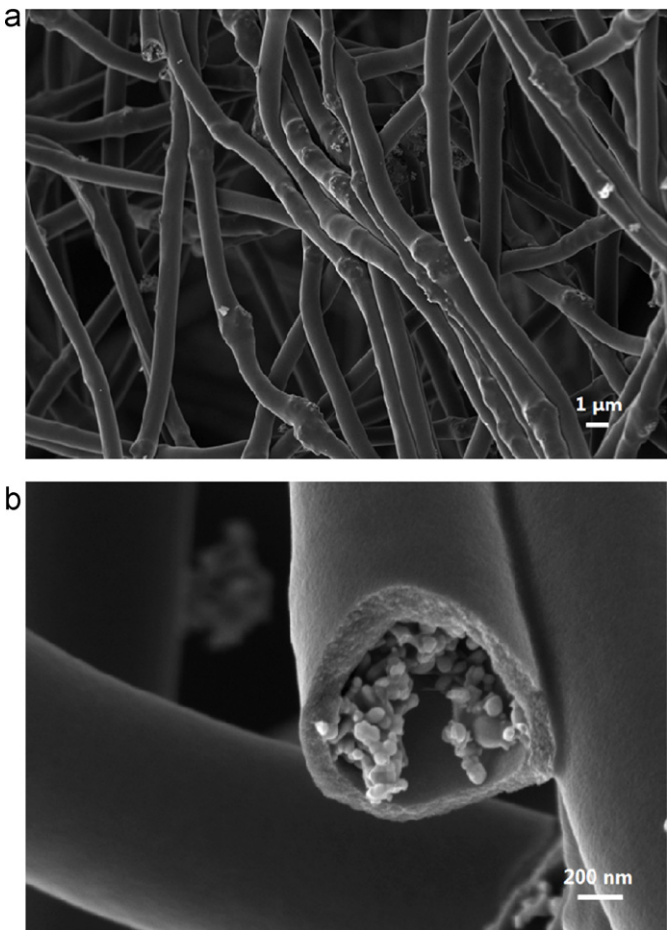

Fig. 2. FE-SEM images of Si core/C shell nanofibers: (a) low and (b) high magnifications.

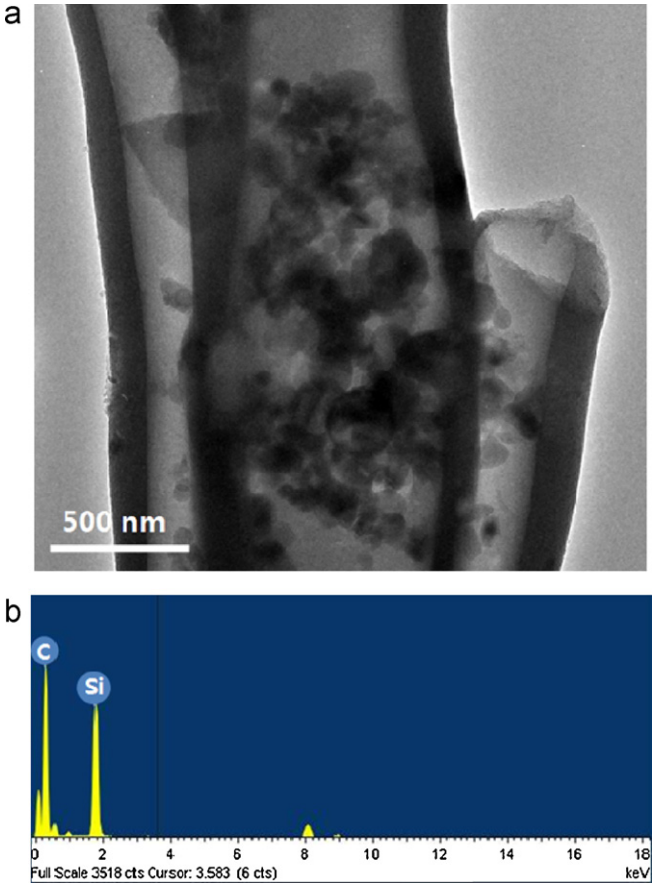

Fig. 3. (a) TEM image of Si core/C shell nanofibers and (b) their EDX profile.

almost the same as that of micro/macro carbonaceous materials [43,44]. Therefore, the current deformation of the C shell during the contact-lithiation is within the affordable range. There are two possible reasons for such C shell expansion: intercalation of Li atoms and volume expansion of the Si core. It is well known that the intercalation of Li atoms into graphite increases the distance between the graphitic layers, for example, 10% extension in the c-axis for perfect graphite and only 3% volume expansion for polycrystalline graphite [45]. Since the C shell in the nanofibers features the turbostratic carbon layers with enlarged d-space (d_{002} = 0.369 nm), Li atoms can intercalate into the carbon layers without inducing further expansion. Furthermore, it is reported that Li intercalation into carbon layers does not bring about any volume or layer expansion [46]. As a result, the expansion of the C shell results most likely from the Si core expansion.

The coarsening of Si core nanoparticles is clearly observable upon the contact-lithiation (see Fig. 6(b)). Their expansions (78% in lengthwise) are bigger than that of the C shell observed above. They are also large compared to theoretically calculated lengthwise change (58.7%) of a Si nanoparticle by assuming isotropic volume expansion (300%) of fully lithiated crystalline Si ($Li_{22}Si_5$) [6,13,47]. This phenomenon probably results from the anisotropic expansion of Si nanoparticles [6]. The C shell is mechanically stable without failure, even though its expansion is not large enough to accommodate such huge expansion of Si nanoparticles. This can be explained by the sparse arrangement of the Si-lumps in Fig. 3(a), which alleviates the stress transferred to the C shell by the expansion of Si nanoparticle. It can be concluded that the C shell accommodates the expansion of Si core nanoparticles caused by lithiation and thus minimize the pulverization and electrical contact loss of Si.

3.3. Electrochemical performance

Galvanostatic charge–discharge tests are conducted to evaluate the electrochemical performance of the Si core/C shell nanofibers. Fig. 8 shows the differential capacity curves of the composite nanofiber anode for the first five cycles between 0.01 and 1.5 V at a current of 50 mA g^{-1}. Hysteresis is not observed during these initial stages of the cycling test except the first one. The Si core nanoparticles are encapsulated at only 9.9 wt.% in

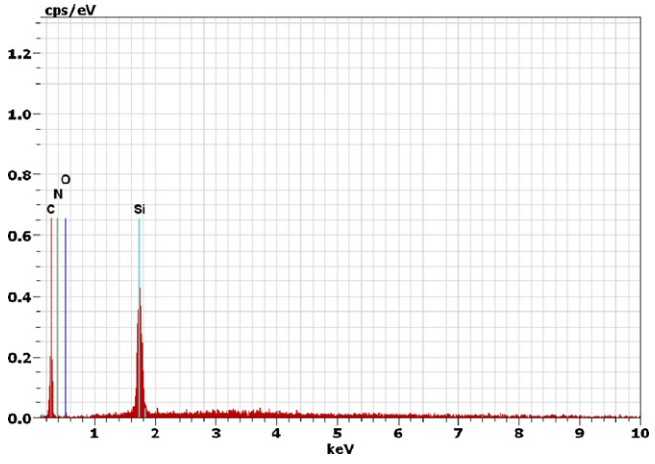

Fig. 4. EDX profile of Si core/C shell nanofibers from FE-SEM.

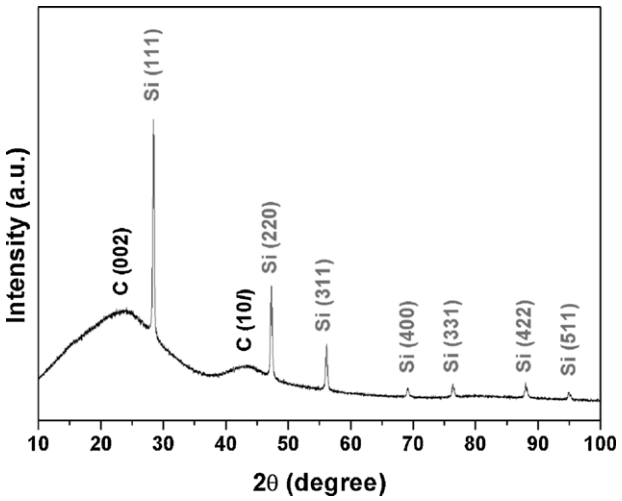

Fig. 5. WAXD pattern of Si core/C shell nanofibers.

the Si core/C shell nanofibers as mentioned in Section 3.1, however their contribution to the overall capacity is considerable. On the first charging, a broad peak is developed at around 0.75 V, which is related to the formation of SEI layers. Note that carbon and Si are known to form SEI at 0.75 and 0.62 V, respectively. The duplicated peak below 0.2 V indicates both the amorphization of the crystalline Si core by the lithiation and the reversible lithiation of the turbostratic C shell [36,48,49]. From the second charging, several peaks related to the lithiation of amorphous Si are significantly developed: 0.24 and 0.09 V during charging and 0.33 V (only for first cycle), 0.27 and 0.44 V during discharging [48]. The reversible charge and discharge behavior of the C shell are shown at below 0.1 and 0.09 V, respectively [36]. All these electrochemical behavior in Fig. 8 supports independent electrochemical reaction of the Si core and C shell.

Fig. 9 shows the cycling electrochemical performance of the Si core/C shell nanofibers. Fig. 9(a) displays the voltage profiles after 1st, 5th, 10th, 15th, and 30th cycles. As expected from Fig. 8, they show no hysteresis throughout the 30 repeated cycles. It can be also seen clearly that the Si core and the C shell independently react to Li-ions without any chemical reaction between Si and C. The initial charge capacity (967 mAh g^{-1}) is higher than the theoretical one (752 mAh g^{-1}), while the reversible capacity is 596 mAh g^{-1}. The reversible capacity of only Si core can be calculated to be 2817 mAh g^{-1} based on the measured reversible capacity of the Si core/C shell nanofibers (596 mAh g^{-1}), the measured reversible capacity of pure hollow carbon nanofibers (352 mAh g^{-1} [36]), and its weight fraction (9.9 wt.%). The huge capacity of only Si core advocates that increased Si nanoparticles outcome naturally higher specific capacity. Meanwhile, the initial coulombic efficiency is improved from 53.9% (pure hollow carbon nanofibers [36]) to 61.6%. Fig. 9 shows the stable cycling performance of the Si core/C shell nanofibers. Their capacity is maintained at around 590 mAh g^{-1} upto 50 cycles with little degradation. The capacity retention is as high as 92% after 50 cycles, and the coulombic efficiency reaches 97.3% at the 5th cycle and is maintained at 98% after the 10th cycle. It can be concluded that the electrochemical performances of the composite anode are significantly improved by incorporating Si nanoparticles in the core of hollow carbon nanofibers, i.e., by fabricating Si core/C shell nanofibers.

Although the previous reports on core/shell structured Si–C anodes have demonstrated the outstanding performances (e.g., Cui et al. demonstrated overwhelmingly electrochemical performances with a specific capacity and a columbic efficiency of ~2000 mAh g^{-1} and 98%, respectively, by using vapor grown method and amorphous silicon phase [27], while Huang et al. made a super anode with the first discharge capacity of 3344 mAh g^{-1} by

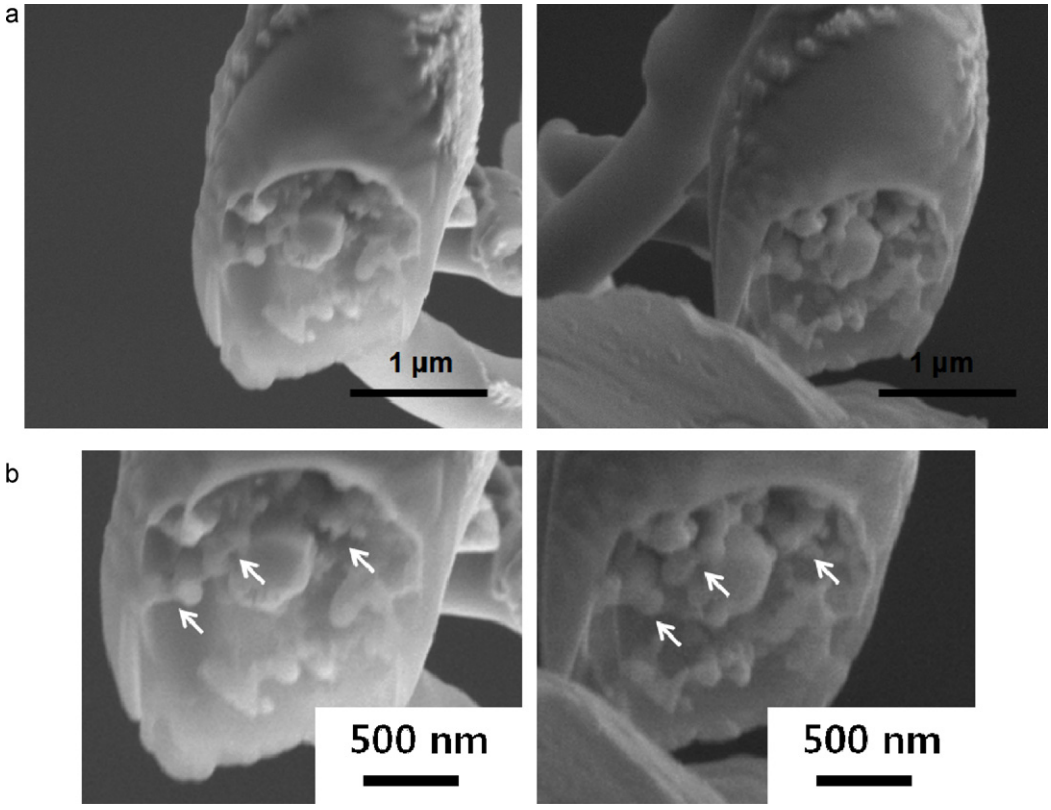

Fig. 6. SEM images of a Si core/C shell nanofiber before (left) and after (right) in situ contact-lithiation: (a) low and (b) high magnification.

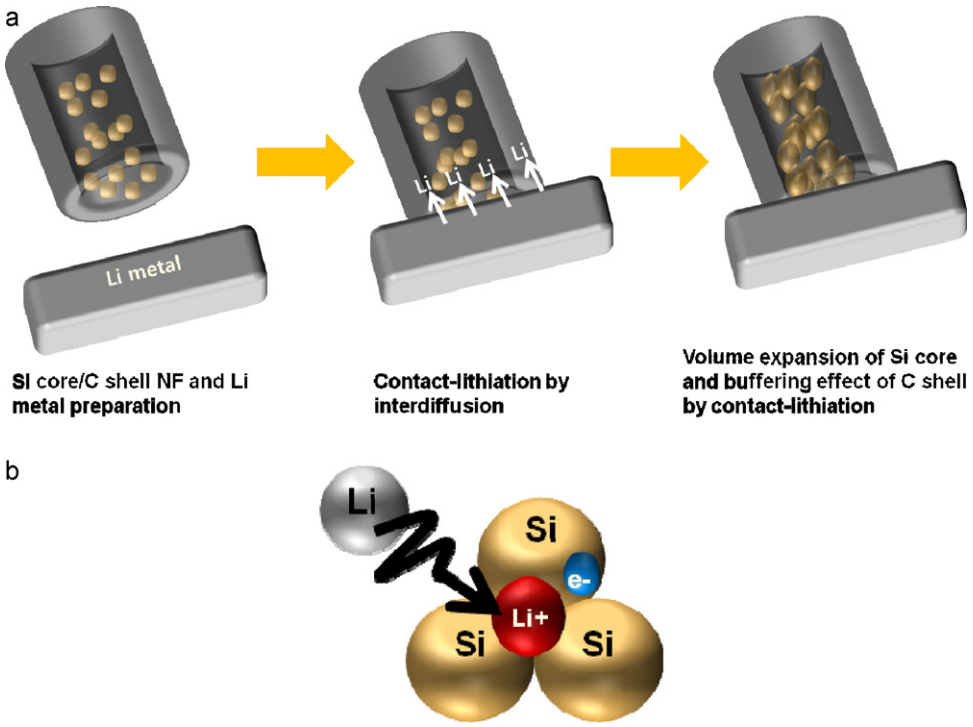

Fig. 7. Schematic diagrams of: (a) volume expansion behavior during contact-lithiation and (b) ionization of Li atom in Si matrix.

etching silicon wafers catalytically and pyrolyzing carbon aerogel [16]), their anodes were not prepared using slurry casting (the conventional method to evaluate the electrochemical performance), which is probably due to low productivity. The massive productivity is, however, embodied in this work. Therefore, the co-axial electrospinning and subsequent thermal treatment is more fascinate in the commercialization point of view. Meanwhile, Sn core/C shell nanofibers were reported with their reversible specific capacity of ~800 mAh g^{-1} where the ratio of Sn and C was 7:3 [33]. Even though the Sn fraction is high, the specific capacity of the nanofibers is not comparable to Si related anodes above, which is mainly due to low capacity (990 mAh g^{-1}) of Sn itself. Here this work aims to utilize huge capacity (4200 mAh g^{-1}) of Si being incorporated into the carbon shell. The current Si core/C shell nanofibers show lower capacity than Sn core/C shell nanofibers do, in particular due to low fraction of Si. Increased Si fraction, however, is expected to enhance the electrochemical performance of the Si core/C shell nanofibers, which will be reported in a future study. Furthermore, comprehensive research efforts should be driven toward developing energy efficient process to facilitate commercialization of the current material.

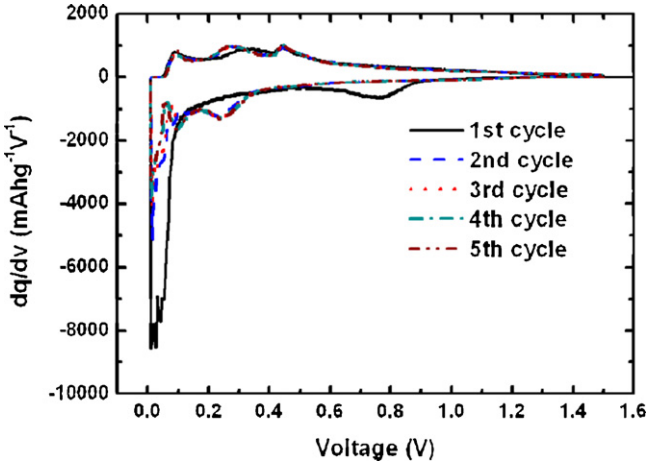

Fig. 8. Differential capacity curve of Si core/C shell nanofibers for the first 5 cycles.

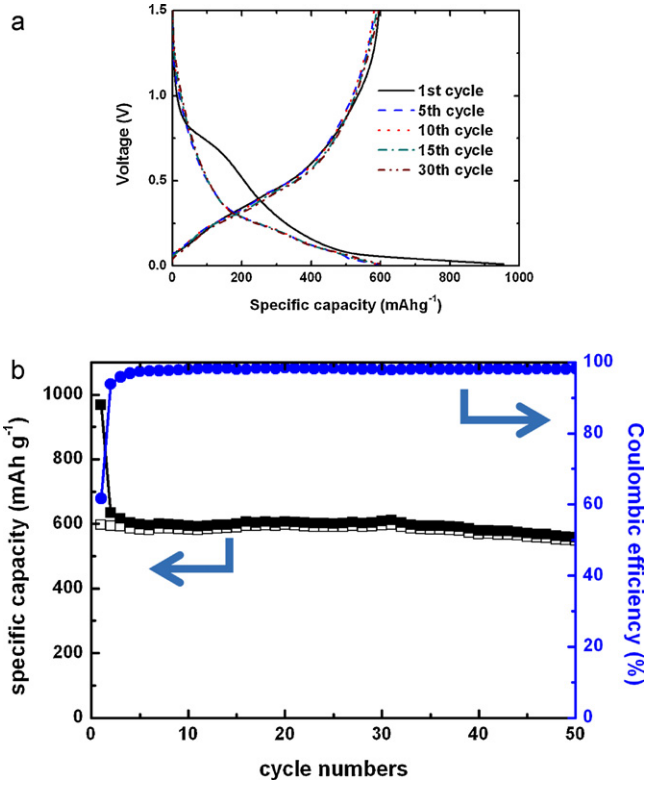

Fig. 9. Cycling performances of Si core/C shell nanofibers: (a) Voltage profiles of Si core/C shell nanofibers after 1st, 5th, 10th, 15th, and 30th cycles and (b) capacity-coulombic efficiency-cycle number curve.

4. Conclusions

Si core/C shell nanofibers have been successfully fabricated using co-axial electrospinning and subsequent thermal treatment. The morphological and crystallographic analyses confirm that the nanofibers have definite Si core and C shell layers without any chemical reaction between these components. In situ observation of the contact-lithiation shows that the mechanical durability of the C shell and Si nanoparticle is ensured during the lithiation, enabling stable electrochemical performance of the Si core/C shell nanofibers. The Si core and C shell components react to Li-ions in a stable and independent manner during the charge–discharge cycles. A considerable improvement ($244\,mAh\,g^{-1}$) in the reversible capacity is achieved by encapsulating Si of 9.9 wt.% into hollow carbon nanofibers. The capacity retention is 92% after 50 cycles and the coulombic efficiency is converged to 98% after 10 cycles.

Acknowledgement

This research was supported by Basic Science Research Program through the National Research Foundation of Korea (NRF) funded by the Ministry of Education, Science and Technology (2010-0022633).

Appendix A. Supplementary data

Supplementary data associated with this article can be found, in the online version, at doi:10.1016/j.jpowsour.2012.01.120.

References

[1] T. Song, J. Xia, J.-H. Lee, D.H. Lee, M.-S. Kwon, J.-M. Choi, J. Wu, S.K. Doo, H. Chang, W.I. Park, D.S. Zang, H. Kim, Y. Huang, K.-C. Hwang, J.A. Rogers, U. Paik, Nano Letters 10 (2010) 1710–1716.
[2] S.-B. Son, J.E. Trevey, H. Roh, S.-H. Kim, K.-B. Kim, J.S. Cho, J.-T. Moon, C.M. DeLuca, K.K. Maute, M.L. Dunn, H.N. Han, K.H. Oh, S.-H. Lee, Advanced Energy Materials 1 (2011) 1199–1204.
[3] K. Peng, J. Jie, W. Zhang, S.T. Lee, Applied Physics Letters 93 (2008) 033105.
[4] Q. Zhang, W. Zhang, W. Wan, Y. Cui, E. Wang, Nano Letters 10 (2010) 3243–3249.
[5] H. Kim, M. Seo, M.-H. Park, J. Cho, Angewandte Chemie International Edition 49 (2010) 2146–2149.
[6] X.H. Liu, H. Zheng, L. Zhong, S. Huang, K. Karki, L.Q. Zhang, Y. Liu, A. Kushima, W.T. Liang, J.W. Wang, J.-H. Cho, E. Epstein, S.A. Dayeh, S.T. Picraux, T. Zhu, J. Li, J.P. Sullivan, J. Cumings, C. Wang, S.X. Mao, Z.Z. Ye, S. Zhang, J.Y. Huang, Nano Letters 11 (2011) 3312–3318.
[7] X.H. Liu, L.Q. Zhang, L. Zhong, Y. Liu, H. Zheng, J.W. Wang, J.-H. Cho, S.A. Dayeh, S.T. Picraux, J.P. Sullivan, S.X. Mao, Z.Z. Ye, J.Y. Huang, Nano Letters 11 (2011) 2251–2258.
[8] S.W. Lee, M.T. McDowell, J.W. Choi, Y. Cui, Nano Letters 11 (2011) 3034–3039.
[9] H. Kim, B. Han, J. Choo, J. Cho, Angewandte Chemie 120 (2008) 10305–10308.
[10] T. Jiang, S. Zhang, X. Qiu, W. Zhu, L. Chen, Electrochemistry Communications 9 (2007) 930–934.
[11] Y. Yao, M.T. McDowell, I. Ryu, H. Wu, N. Liu, L. Hu, W.D. Nix, Y. Cui, Nano Letters 11 (2011) 2949–2954.
[12] C.K. Chan, R.N. Patel, M.J. O'Connell, B.A. Korgel, Y. Cui, ACS Nano 4 (2010) 1443–1450.
[13] C.K. Chan, H. Peng, G. Liu, K. McIlwrath, X.F. Zhang, R.A. Huggins, Y. Cui, Nature Nanotechnology 3 (2008) 31–35.
[14] M.-H. Park, M.G. Kim, J. Joo, K. Kim, J. Kim, S. Ahn, Y. Cui, J. Cho, Nano Letters 9 (2009) 3844–3847.
[15] L.-F. Cui, R. Ruffo, C.K. Chan, H. Peng, Y. Cui, Nano Letters 9 (2008) 491–495.
[16] R. Huang, X. Fan, W. Shen, J. Zhu, Applied Physics Letters 95 (2009) 133119.
[17] H. Kim, J. Cho, Nano Letters 8 (2008) 3688–3691.
[18] R. Krishnan, T.-M. Lu, N. Koratkar, Nano Letters 11 (2010) 377–384.
[19] A. Magasinski, P. Dixon, B. Hertzberg, A. Kvit, J. Ayala, G. Yushin, Nature Materials 9 (2010) 353–358.
[20] X.-W. Zhang, P.K. Patil, C. Wang, A.J. Appleby, F.E. Little, D.L. Cocke, Journal of Power Sources 125 (2004) 206–213.
[21] J.K. Lee, K.B. Smith, C.M. Hayner, H.H. Kung, Chemical Communications 46 (2010) 2025–2027.
[22] M. Miyachi, H. Yamamoto, H. Kawai, T. Ohta, M. Shirakata, Journal of the Electrochemical Society 152 (2005) A2089–A2091.
[23] T. Song, D.H. Lee, M.S. Kwon, J.M. Choi, H. Han, S.G. Doo, H. Chang, W.I. Park, W. Sigmund, H. Kim, U. Paik, Journal of Materials Chemistry 21 (2011) 12619–12621.
[24] Z.P. Guo, E. Milin, J.Z. Wang, J. Chen, H.K. Liu, Journal of the Electrochemical Society 152 (2005) A2211–A2216.
[25] L. Ji, X. Zhang, Electrochemistry Communications 11 (2009) 1146–1149.
[26] L. Ji, X. Zhang, Carbon 47 (2009) 3219–3226.
[27] L.-F. Cui, Y. Yang, C.-M. Hsu, Y. Cui, Nano Letters 9 (2009) 3370–3374.
[28] L. Wang, C.X. Ding, L.C. Zhang, H.W. Xu, D.W. Zhang, T. Cheng, C.H. Chen, Journal of Power Sources 195 (2010) 5052–5056.
[29] L. Ji, Z. Lin, A.J. Medford, X. Zhang, Chemistry: A European Journal 15 (2009) 10718–10722.
[30] L. Ji, X. Zhang, Energy and Environmental Science 3 (2010) 124–129.
[31] L. Ji, X. Zhang, Nanotechnology 20 (2009) 155705.
[32] L. Ji, X. Zhang, Electrochemistry Communications 11 (2009) 795–798.
[33] Y. Yu, L. Gu, C. Wang, A. Dhanabalan, P.A. van ssAken, J. Maier, Angewandte Chemie International Edition 48 (2009) 6485–6489.
[34] B. Sun, B. Duan, X. Yuan, Journal of Applied Polymer Science 102 (2006) 39–45.
[35] B. Liu, Y. Yu, J. Chang, X. Yang, D. Wu, X. Yang, Electrochemistry Communications 13 (2011) 558–561.
[36] B.-S. Lee, S.-B. Son, K.-M. Park, W.-R. Yu, K.-H. Oh, S.-H. Lee, Journal of Power Sources 199 (2012) 53–60.
[37] Y.S. Jung, S. Lee, D. Ahn, A.C. Dillon, S.-H. Lee, Journal of Power Sources 188 (2009) 286–291.
[38] M.S.A. Rahaman, A.F. Ismail, A. Mustafa, Polymer Degradation and Stability 92 (2007) 1421–1432.
[39] Q. Si, K. Hanai, T. Ichikawa, A. Hirano, N. Imanishi, Y. Takeda, O. Yamamoto, Journal of Power Sources 195 (2010) 1720–1725.
[40] A. Ōya, H. Marsh, Journal of Materials Science 17 (1982) 309–322.
[41] H. Reiss, The Journal of Chemical Physics 25 (1956) 681–686.
[42] M. Holzapfel, H. Buqa, L.J. Hardwick, M. Hahn, A. Würsig, W. Scheifele, P. Novák, R. Kötz, C. Veit, F.-M. Petrat, Electrochimica Acta 52 (2006) 973–978.
[43] S.N. Arshad, M. Naraghi, I. Chasiotis, Carbon 49 (2011) 1710–1719.
[44] J.C. Chen, I.R. Harrison, Carbon 40 (2002) 25–45.
[45] L. Zou, F. Kang, X. Li, Y.-P. Zheng, W. Shen, J. Zhang, Journal of Physics and Chemistry of Solids 69 (2007) 1265–1271.
[46] I. Lahiri, S.-W. Oh, J.Y. Hwang, S. Cho, Y.-K. Sun, R. Banerjee, W. Choi, ACS Nano 4 (2010) 3440–3446.
[47] S.H. Ng, J. Wang, D. Wexler, S.Y. Chew, H.K. Liu, The Journal of Physical Chemistry C 111 (2007) 11131–11138.
[48] C.K. Chan, R. Ruffo, S.S. Hong, R.A. Huggins, Y. Cui, Journal of Power Sources 189 (2009) 34–39.
[49] J.S. Kim, Y.T. Park, Journal of Power Sources 91 (2000) 172–176.